DETERMINATION OF THE LATERAL RESOLUTION OF AN INTERFERENCE MICROSCOPE USING A MICRO-SCALE SPHERE

Rong Su[1], Matthew Thomas[1], Peter de Groot[2], Jeremy Coupland[3], Richard Leach[1]
[1]Manufacturing Metrology Team, Faculty of Engineering, University of Nottingham, Nottingham NG8 1BB, UK
[2]Zygo Corporation, Middlefield, Connecticut, USA
[3]Wolfson School of Mechanical, Electrical and Manufacturing Engineering, Loughborough University, Loughborough LE11 3TU, UK

INSTRUCTION

The lateral resolution of a surface topography measuring instrument refers to the ability to clearly distinguish surface heights between two closely spaced features. Specifications for lateral resolution often include the traditional Rayleigh and Sparrow criteria inherited from optical imaging systems [1], and there are more definitions that include a measure of the height transmission listed in the draft ISO specification standard, ISO 25178 part 600 [2].

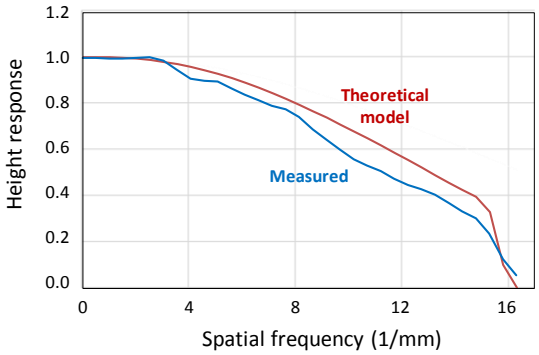

FIGURE 1 Example instrument transfer function of a laser Fizeau interferometer showing a spatial frequency limit of 16 cycles/mm over a 100 mm aperture [3].

A more complete characterisation of lateral resolution is the linear height-response instrument transfer function (ITF). The linear ITF represents the measured amplitudes relative to the true amplitudes of surface sine waves as a function of spatial frequency. In the limit of low-amplitude sine waves ($<<\lambda/4$), we can predict the instrument response by mapping the Fourier components of the surface, weighted by the ITF, to the surface topography. The small height limitation in the ITF representation follows from the need to avoid nonlinear effects and to keep the spatial frequencies separable [1].

FIGURE 1 shows the measured ITF for a laser Fizeau interferometer [3]. Data of this kind are valuable when using optical metrology to quantify the power spectral density of a surface – an important parameter in optics fabrication.

There are a variety of calibration artefacts for lateral resolution, such as a line pairs, star patterns, a series of sinusoids with a chirped pitch and pseudo-random binary structures [4]. The measurement results in FIGURE 1 correspond to a line-spread function test, using a 30 nm step feature [3].

An alternative to directly measuring the ITF over a range of surface frequencies is to calculate the ITF using modelling. The theoretical curve in FIGURE 1, for example, follows from a Fourier optics analysis of a coherent system, including apertures and known aberrations, with the object represented as a distribution of phase shifts proportional to surface heights [5]. Once this model is in place, for the purpose of generating a height-response ITF, it is easy enough to generate virtual sinusoidal surfaces in software at the small ($<\lambda/4$) surface height limit.

The modelling approach to the ITF presupposes that we have an effective means of calibrating for the optical properties of the instrument. This becomes increasingly cumbersome for techniques such as coherence scanning interferometry (CSI), which employs a spatially-extended, spectrally-broadband light source [6]. Modelling of such systems traditionally involves diffraction calculations followed by numerical integration over an area of pupil positions, illumination directions and optical path lengths for each point in the field of view, under the assumption of ideal optics [7,8].

A compelling modelling framework for surface topography measurement using CSI relies on the

definition of a 3D transfer function (3D TF) for the optical system [9-11]. In this framework, the object surface is a weakly-scattering structure or "foil", and under reasonable physical conditions, we can compactly model the CSI imaging process as a 3D linear shift-invariant filtering operation. This linear systems theory is valid provided two assumptions are satisfied: 1) the first Born approximation is assumed, which means the total electromagnetic field on the surface is only determined by the incident field [12]. This approximation is accurate if the scattered field is small compared to the incident field on the surface. The weak scattering case can be considered when the refractive index contrast is small or if the object consists of sparse point-like objects. 2) Alternatively, the foil model of the surface must be valid, where the surface can be strongly scattering but must be slowly varying on a wavelength scale, i.e. the radius of the local curvature of the surface is much greater than a wavelength, such that the multiple scattering effect is negligible and the Kirchhoff approximation is assumed. Moreover, the reflection coefficient is assumed constant and polarisation independent over the range of incident/reflected angles accepted by the numerical aperture (NA) [13]. The Kirchhoff approximation is required if the refractive index contrast is large between the air and the material.

Importantly, based on the foil model of the surface, it is possible to fully characterise the transfer properties and the resolutions of a CSI system by measuring a precision sphere [14-16]. This follows from the observation that a sphere, which is smaller than the field of view, reflects light through all possible angles within the NA limits of the optics. Once this calibration is completed, it is straightforward to calculate what the response would be to a sequence of sinusoids of small amplitudes, providing the height-response ITF.

In this paper, we will demonstrate calculation of the linear height-response ITF of a CSI system using the foil model, calibrated using a precision sphere. This approach provides an alternative to calibration by the more familiar specimens, such as star patterns and chirped sinusoids, while enabling a more complete system characterisation than the traditional ITF specification.

METHOD

CSI is a well-established technique for surface topography measurement [17,18]. The major advantage of CSI is that it can estimate the phase information of the light back-reflected/scattered from the sample surface and the spectrum of broadband light source modulates the interferometric fringes in order to make it easier to determine the fringe order than in traditional phase shifting interferometry. CSI overcomes the 2π ambiguity that can be present when the surface topography or a sharp step feature interrupts the imaging of continuous interference fringes.

The detailed theoretical derivation of the foil model and the characterisation of the 3D TF of CSI can be found elsewhere [10,14,19]. Here, we will briefly describe the characterisation procedure. As shown in FIGURE 2, we first acquire the 3D fringe data of the spherical cap by CSI data acquisition and storing the intensity image stack in the usual way. Given that the sphere diameter is known, the foil function of the spherical cap, described as

$$o(x,y,z) = 4\pi jRw(x,y)\delta[z - s(x,y)], \quad (1)$$

where $j = \sqrt{-1}$, R is the Fresnel amplitude reflection coefficient and is assumed to be a complex constant for simplicity, corresponding to the limit case of normal incidence reflection [10], and $w(x,y)$ is a window function with smooth cut-off for defining the space-limited surface region under illumination. The 'foil' is defined by the 1D Dirac delta function $\delta(z)$ based on the surface topography of the object $s(x,y)$. The foil function can be generated numerically. Taking the Fourier transform of the fringe data and the foil function gives us the spectra of the spatial frequency components. Then the 3D TF for the specific optical instrument at the time of calibration can be calculated by dividing the fringe by the foil in the spatial frequency domain. From the 3D TF, the point spread function (PSF) can be derived through its inverse Fourier transform, and the 2D TF is calculated as the projection of the 3D TF onto the *x*-*y* plane by summing the 3D TF along the axial direction for each lateral spatial frequency. The 1D ITF plot, similar to FIGURE 1, can then be extracted from the 2D TF. In other words, the traditional ITF can be obtained by dimension reduction of the 3D TF.

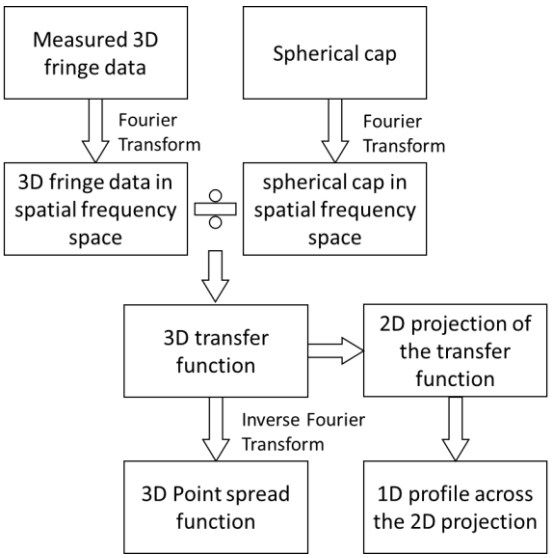

FIGURE 2 Characterisation procedure of 3D TF of CSI.

In this work, we use a ZYGO NewView™ 8300 CSI system with a 0.55 NA objective lens, 167 µm field of view and 0.163 µm lateral sampling distance. The three microspheres used here are made of silica and have different diameters, 44 µm, 57 µm and 59 µm. The spheres are checked for surface quality and sphericity under scanning electron microscope (SEM) as shown in FIGURE 3, and we assume the sphericity error is negligible, i.e. the sphere can be described solely by its diameter. More information about the necessary microsphere tolerance is given elsewhere [15].

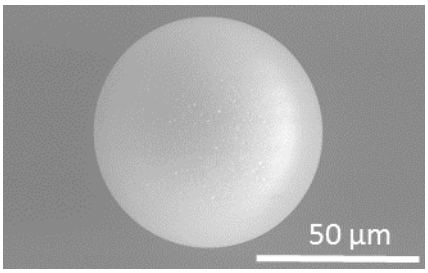

FIGURE 3 SEM image of a microsphere.

RESULTS

The three microspheres of different diameters were measured with CSI, and the 3D fringe data for each obtained. As previously mentioned, we compute a 3D TF from each measurement, where each sphere's diameter determines the form of each modelled surface. For each sphere, measurements are taken at four orientations (0°, 90°, 180°, 270°). The resulting TFs from each orientation are averaged to reduce the effect of any directional bias, such as those caused by asphericity of the microsphere or the influence of randomly located dust particles on the spherical surface. This averaging is performed by taking the arithmetic mean of the magnitude of differently orientated 3D TFs. The result of this can be seen in FIGURE 4.

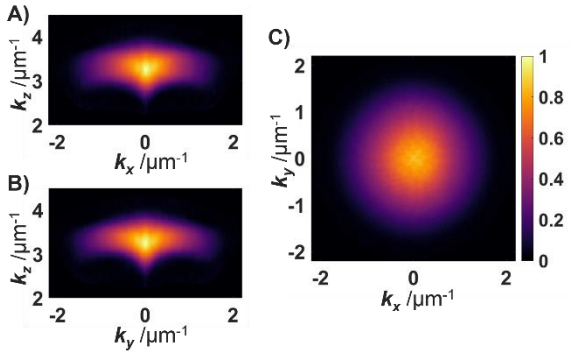

FIGURE 4 Magnitude of the 3D TF associated with the 44 µm sphere after averaging and normalisation to one. Slices are shown at spatial frequencies A) k_y = 0, B) k_x = 0, and C) k_z =2/λ= 3.45 µm^{-1} (λ = 0.58 µm). The colour bar and colour map used are shared between the three slices.

A 3D PSF is acquired by the inverse Fourier transform of the 3D TF, and is displayed in FIGURE 5. It is interesting to note that the 3D PSF of CSI contains fringes along the axial direction, which would not be seen in an ordinary widefield microscope.

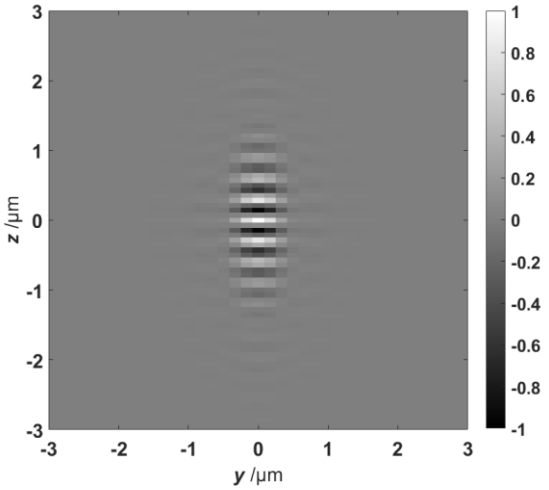

FIGURE 5 A slice of the 3D PSF, computed by inverse Fourier transform of the 3D TF shown in FIGURE 4. Magnitude normalised to one for plotting.

The averaged 3D TF of each sphere is projected onto the lateral spatial frequency (k_x-k_y) plane to produce a 2D projection of the 3D TF. This process is done by summing the 3D TF along the k_z direction at each k_x and k_y, followed by

normalising the magnitude of the resulting 2D projection to one. This projection characterises at each lateral spatial frequency coordinate (k_x,k_y) the instrument's ability to transfer the surface function (equation (1)) to the measured optical field (i.e. the 3D fringe data). From the fringe data, the surface topographic information is retrieved using a surface reconstruction algorithm, e.g. the frequency domain analysis method [20].

From each of the averaged 3D TFs we obtain an approximately circularly-symmetric 2D projection (which is what we would expect from an optical imaging system with a circular aperture). The one shown in FIGURE 6 is obtained from the 44 µm sphere. The 3D TFs and the corresponding 2D projections obtained from the measurements of the three spheres are almost completely identical to each other, despite the differences in diameter between the three spheres, providing evidence that the transfer function of a CSI can be obtained solely via measurement of a microsphere based on the linear theory of CSI.

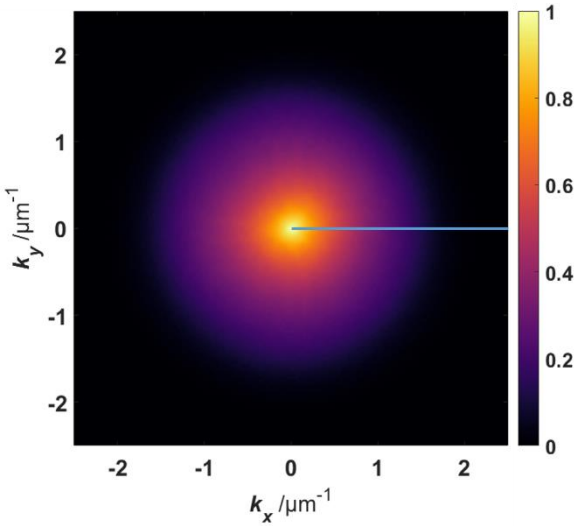

FIGURE 6 The 2D projection of the 3D TF shown in FIGURE 4. Since the other two projections associated with the other two spheres are nearly identical, only one is displayed. The blue lines are the lines along which profiles are taken for FIGURE 7.

Profiles of the three projections are taken radially from the origin of the axes, in this case arbitrarily along the positive k_x axis (marked in FIGURE 6), and compared to both each other and the theoretical model in FIGURE 7. This theoretical model is produced using equation (32) in reference [10]. Given the system has a 0.55 NA, the central wavelength of 0.58 µm and full-width-at-half-maximum bandwidth of 0.08 µm, the theoretical cut-off frequency is approximately 2 µm^{-1}.

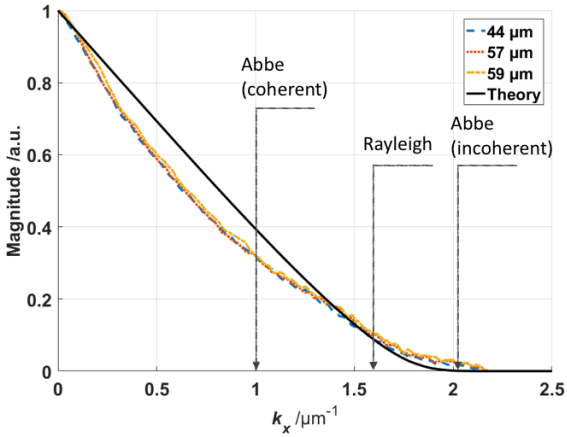

FIGURE 7 Profiles of the 2D projections from each sphere measurement taken along the positive k_x axis as marked on FIGURE 6. The projection associated with the 44 µm diameter sphere is the blue dashed line, the 57 µm is the red dotted line, the 59 µm is the yellow dash-dot line, and the theoretical model is given by the black solid line. Cut-off frequencies corresponding to the Rayleigh and Abbe criteria of resolution limit are shown.

The measured TFs are in general very close to the theoretical one. The discrepancy is highly likely caused by slight defocus of the CSI system. The reader may consult [16] for more detailed explanation and discussion on this. Assuming the surface reconstruction algorithm is a linear operation applied to the measured optical field and the digital sampling frequency of the camera is higher than 2 µm^{-1} (which is true for high magnification objective lens), the traditional ITF defined in [1] can be estimated from the 3D TF.

CONCLUSION

The linear height-response instrument transfer function (ITF) offers a more complete characterisation of the lateral resolution of an optical surface topography measuring instrument. We demonstrate in this paper, the ITF can be estimated from measuring a microsphere based on the linear theory of 3D imaging, particularly in this case, the foil model in CSI. This approach provides an alternative to calibration by the more familiar specimens such as star patterns and chirped sinusoids.

Importantly, an optical model such as the 3D TF presented here is not limited to recreating the linear ITF, which is known to have limitations based on the assumption of linear response of the

instrument [1]. The foil model provides a means of predicting the response to more challenging surface topographies and shapes that often give rise to anomalous or unexpected results that are inconsistent with the linear response. The sphere calibration, therefore, enables a more complete system characterisation than the traditional ITF specification, potentially leading to software correction methods to extend the linear range of the instrument [14,19]. For future work, the authors will provide a rigorous experimental verification of the foil model and investigate the validity regimes of the ITF and 3D TF, and their relationship.

ACKNOWLEDGEMENT

This work was supported by the Engineering and Physical Sciences Research Council (EPSRC) (EP/M008983/1) and the European Metrology Programme for Innovation and Research (EMPIR) project FreeFORM (15SIB01).

REFERENCES

1. Colonna de Lega X, de Groot P. Lateral resolution and instrument transfer function as criteria for selecting surface metrology instruments. OSA Proc. Optical Fabrication and Testing 2012; OTu1D.
2. ISO 25178-600:2017 Geometrical product specifications (GPS) – surface texture: areal – part 600: Metrological characteristics for areal-topography measuring methods.
3. Deck LL and de Groot P. Using the instrument transfer function to evaluate Fizeau interferometer performance. OSA Technical Digest 2017; OM2B.7.
4. Leach RK, Giusca CL, Haitjema H, Evans C, Jiang X. Calibration and verification of areal surface texture measuring instruments Ann. CIRP 2015; 64: 797-813.
5. Goodman JW. Introduction to Fourier Optics, 3rd edition. Roberts & Company: 2005.
6. de Groot P. Principles of interference microscopy for the measurement of surface topography. Advances in Optics and Photonics 2015; 7: 1-65.
7. Totzeck M. Numerical simulation of high-NA quantitative polarization microscopy and corresponding near-fields. Optik 2001; 112: 399-406.
8. de Groot P, Colonna de Lega X, Liesener J et al. Metrology of optically-unresolved features using interferometric surface profiling and RCWA modelling. Opt. Express 2008; 16: 3970.
9. Coupland JM and Lobera J. Holography, tomography and 3D microscopy as linear filtering operations. Meas. Sci. Technol. 2018; 19: 07010.
10. Coupland JM, Mandal R, Palodhi K, Leach RK. Coherence scanning interferometry: linear theory of surface measurement. Appl. Opt. 2013; 52: 3662-3670.
11. Kou SS and Sheppard CJR. Imaging in digital holographic microscopy. Opt. Express 2007; 15: 13640-13648.
12. Born M and Wolf E. Principles of Optics: Electromagnetic Theory of Propagation, Interference and Diffraction of Light, 7th edition. Cambridge: Cambridge University Press: 1999.
13. Beckmann P and Spizzichino A. The Scattering of Electromagnetic Waves from Rough Surfaces. Pergamon: 1963.
14. Su R, Wang Y, Coupland JM, Leach RK. On tilt and curvature dependent errors and the calibration of coherence scanning interferometry. Opt. Express 2017; 25: 3297-3301.
15. Su R, Coupland JM, Wang Y, Leach RK. Tolerance on sphere radius for the calibration of the transfer function of coherence scanning interferometry. Proc. SPIE 2017; 10329.
16. Su R, Thomas M, Leach RK, Coupland JM. Effects of defocus on the transfer function of coherence scanning interferometry. Opt. Lett. 2018; 43: 82-85.
17. de Groot P. Chapter 9. Coherence scanning interferometry, in Optical Measurement of Surface Topography. Leach RK. Springer: 2011.
18. ISO 25178-604:2013 Geometrical product specifications (GPS) – surface texture: areal – part 604: Nominal characteristics of non-contact (coherence scanning interferometry) instruments.
19. Mandal R, Coupland J, Leach RK, Mansfield D. Coherence scanning interferometry: measurement and correction of three-dimensional transfer and point-spread characteristics. Appl. Opt. 2014; 53: 1554-1563.
20. de Groot P, Deck L. Surface profiling by analysis of white-light interferograms in the spatial frequency domain. J. Mod. Opt. 1995; 42: 389-401.